

# Radial Velocity Variations in Pulsating Ap Stars. II. 33 Librae <sup>★</sup>

D.E. Mkrtichian<sup>1,2</sup>, A.P. Hatzes<sup>3</sup>, & A. Kanaan<sup>4</sup>

<sup>1</sup>*Astrophysical Research Center for the Structure and Evolution of the Cosmos, Sejong University, Seoul 143-747, Korea*

<sup>2</sup>*Astronomical Observatory, Odessa National University, Shevchenko Park, Odessa, 65014, Ukraine*

<sup>3</sup>*Thüringer Landessternwarte Tautenburg, Sternwarte 5, D-07778, Tautenburg, Germany*

<sup>4</sup>*Departamento de Física, Universidade Federal de Santa Catarina, Campus Universitário, 88040-900, Florianópolis, Brazil <sup>†</sup>*

## ABSTRACT

We present precise relative radial velocity (RV) measurements for the rapidly oscillating Ap (roAp) star 33 Librae measured from high resolution data spanning the wavelength interval 5000–6200 Å. We find that pulsational radial velocity amplitude determined over a broad wavelength range ( $\approx 100$  Å) depends on the spectral region that is examined and can be as high as  $60 \text{ ms}^{-1}$  at 5600 Å and as low as  $7 \text{ ms}^{-1}$  in the 5900 Å region. RV measurements of individual spectral lines can show higher amplitudes than results obtained using a “broad-band” measurement that includes many spectral lines. The acoustic cross-sections of the atmosphere, i.e. the phase and amplitude of the pulsations, as a function of optical depth is found for spectral lines of Ca, Cr, Fe, La, Ce, Gd, Er and Nd. This analysis shows that pulsation phase is variable through the atmosphere and that Nd III lines pulsate almost  $180^\circ$  out-of-phase with those of Nd II features and are formed significantly higher in the stellar atmosphere. This conclusively establishes the presence of at least one radial node to the pulsations in the upper stellar atmosphere. We have estimated that this acoustic node is located above an optical depth  $\log \tau < -4.5$  and below the level where the Nd III lines are formed. We also suspect that there may be a second atmospheric node in the lower atmosphere below, or at  $\log \tau \simeq -0.9$  and close to continuum formation level.

The histogram of pulsational phases for all individual spectral feature shows a bi-modal Gaussian distribution with 17% of the lines having a pulsational phase  $\approx 165^\circ$  out-of-phase with most other spectral lines. This is also consistent with the presence of a radial node in the stellar atmosphere. The accumulation of phase due to a running wave component can explain the  $165^\circ$  phase difference as well as the broader width (by a factor of two) of one of the Gaussian components of the phase distribution.

We also found evidence for phase variations as a function of effective Lande g-factors. This may be the influence of magnetic field and magnetic intensification effect on depths of spectral lines formation and that magnetic field is controlling the pulsations. Our RV measurements for 33 Lib suggest that we are seeing evidence of vertical structure to the oscillations as well as the influence of the distribution of elements on the stellar surface. We suggest and briefly discuss a new semi-empirical tomographic procedure for mono- and multi-mode roAp stars that will use acoustic cross-sections obtained on different chemical elements and different pulsation modes for restoring the abundance and acoustic profiles throughout the stellar atmosphere and across the stellar surface.

**Key words:** Stars:individual:33 Lib – Stars:pulsation – Stars:variables

## 1 INTRODUCTION

The rapidly oscillating Ap stars (roAp) are a subclass of the magnetic A stars that pulsate in high order, low-degree modes (see review by Kurtz 1990). Much of our knowledge about the pulsations in roAp stars have come from pho-

tometric studies since the short periods of the oscillations (5–15 min) make it difficult to accumulate the high quality spectral data needed for radial velocity studies. Recently, radial velocity measurements have been made on several roAp stars and these are starting to yield exciting results.

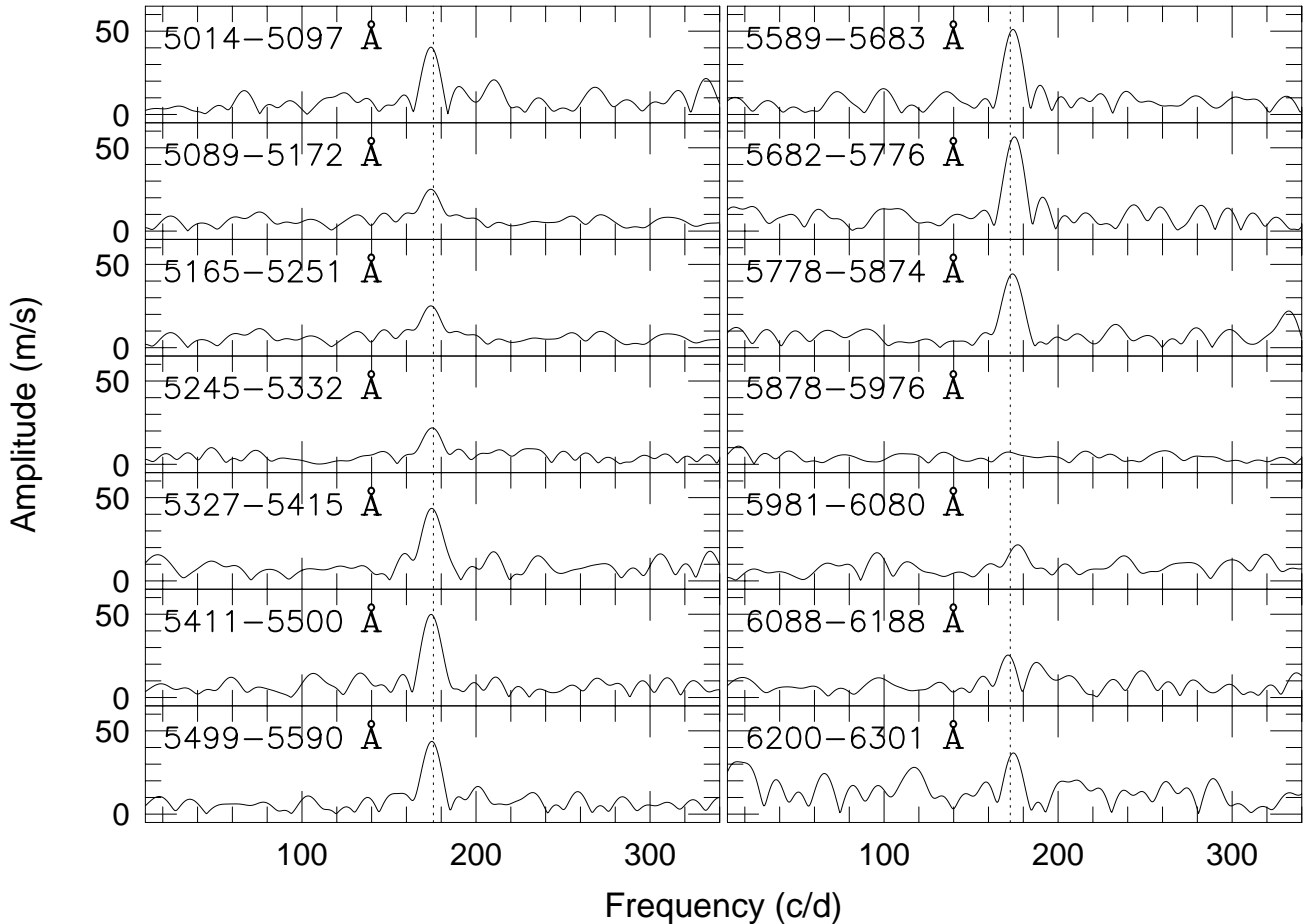


**Figure 1.** The discrete Fourier transform of our RV measurements for 33 Lib. Each panel represents a different spectral order with a wavelength range specified by the numbers in the upper left of each panel. The vertical dashed line is the location of the principal photometric frequency.

Early investigations concentrated merely on detecting radial velocity (RV) variations in roAp stars primarily to confirm that pulsations were indeed responsible for the photometric variations and to measure the RV amplitude-to-photometric amplitude ratio ( $2K/\Delta m$ ) which is useful for comparing to values derived for other pulsating stars. The first successful attempt at measuring the pulsational RV for an roAp star was done for HR 1217 by Matthews et al. (1988). The estimated  $2K$ -amplitude for this star over the wavelength interval 4350 – 4500 Å was about  $400 \text{ m s}^{-1}$  which yielded a  $2K/\Delta m$  of  $59 \pm 12 \text{ km s}^{-1} \text{ mag}^{-1}$ , a value comparable to that found in Cepheid-type variable stars. There was evidence that the RV amplitude varied with rotational phase since observations made on the previous night showed no significant RV variations above an amplitude of  $130 \text{ m s}^{-1}$ . Belmonte et al. (1989) detected RV oscillations in HR 1217 with a frequency of 2.72 mHz and an amplitude of  $258 \pm 60 \text{ m s}^{-1}$ . This yielded a  $2K/\Delta m$  of  $\approx 190 \text{ km s}^{-1} \text{ mag}^{-1}$ , significantly higher than the Matthews et al. (1988) result.

RV measurements at much higher RV precision using a self-calibrating iodine absorption cell were subsequently made for two other roAp stars. Libbrecht (1988) measured an RV amplitude of about  $42 \text{ m s}^{-1}$  in  $\gamma$  Equ based on observations spanning the wavelength interval 5322 – 5377 Å. This

resulted in  $2K/\Delta m = 26 \text{ km s}^{-1} \text{ mag}^{-1}$ . Hatzes & Kürster (1994) placed an upper limit of  $23 \text{ m s}^{-1}$  to any RV variations of the roAp star  $\alpha$  Cir based on spectral data spanning the wavelength interval 5365 – 5410 Å. This yielded  $2K/\Delta m < 10 \text{ km s}^{-1} \text{ mag}^{-1}$ .

More detailed studies of roAp stars have established that the pulsational RV behavior for these stars can be quite complex with measured RV amplitudes differing by factors of 10–100 for the same star depending on the spectral region that is examined. In contrast to the low amplitude measured by Hatzes & Kürster (1994), Baldry et al. (1998) measured the RV pulsational amplitude for  $\alpha$  Cir and found that this was as high as  $1 \text{ km s}^{-1}$  in some spectral regions. Furthermore, those spectral regions dominated by strong lines had a lower pulsational RV amplitude than weaker spectral lines.

Kanaan & Hatzes (1998; hereafter Paper I) presented RV measurements for  $\gamma$  Equ derived using a number of spectral lines which showed that the pulsational RV amplitude depended not only on line strength, but on atomic species as well. Since weaker spectral lines are formed, on average, deeper in the stellar atmosphere the amplitude variations found in Paper I were interpreted as an atmospheric height effect resulting from a radial node situated in the stellar atmosphere. The line-by-line RV measurements for  $\gamma$  Equ with more limited temporal and wavelength coverage by

Kochukov & Ryabchikova (2001) confirmed the strong dependence of pulsation amplitudes from atomic species and phase differences for different elements and stages of ionization.

In retrospect these large variations in the measured value of  $2K/\Delta m$  in roAp stars are not surprising. Mkrtichian (1992) first noted that the spotty distribution of elements on roAp stars would greatly affect the measurement of the RV amplitude and consequently the RV-to-photometric amplitude ratio. A  $2K/\Delta m$  determination for roAp stars would be meaningless since it would depend on the spectral lines used for the RV determination. This seems to be confirmed by recent RV studies of these stars.

Baldry et al. (1998) found that approximately 15% of the wavelength bands they examined in  $\alpha$  Cir showed a  $180^\circ$  phase shift to other bands. One explanation of such a bi-modal distribution is a horizontal node effect due to the inhomogeneous surface distribution of elements (Mkrtichian 1992, 1994). Alternatively, this bi-modal distribution in phases can result from different lines pulsating in opposite phases across a vertical atmospheric radial node (Baldry et al. 1998). The later is consistent with the amplitude variations in line strength found by Kanaan & Hatzes (1998) and the decline in photometric amplitude with increasing wavelength (Medupe & Kurtz 1998). Although these studies are suggestive of the presence of such a wave, this is not conclusive. Furthermore it may be difficult to disentangle the effects of the vertical standing waves to those due to the horizontal surface amplitude distributions of non-radial pulsations (NRP). Mkrtichian et al. (2000) suggested separating the horizontal and vertical atmospheric effects by using spectral lines that are formed at different atmospheric heights and that have a different horizontal abundance distribution across the stellar surface. Understanding the pulsations in roAp stars is indeed challenging, but the rewards may be great in that we could derive important information about the 3-dimensional structure (vertical and horizontal) of the pulsations. RV measurements will play a key role in such studies.

We have started a program to use precise RV measurements to study the pulsations in roAp stars. This program has already detected “broad-band” (i.e. computed over a large wavelength range) RV variations in the roAp stars HD 134214, HR 1217 (Hatzes et al. 1999a; Hatzes et al. 2002), 33 Lib (Hatzes et al. 1999b), and HD 122970 (Hatzes et al. 2000). A line-by-line analysis using high resolution ( $R(=\lambda/\Delta\lambda) > 45,000$ ) data covering a wide wavelength range has been made for relatively few roAp stars. If we are to understand the influence of the magnetic field, surface distribution of elements, and atmospheric structure on the characteristics of the pulsational RV variations then we must make these kinds of measurements for more of roAp stars spanning the available parameter space covered by these stars. Here we present a time series of precise RV measurements, both broad-band and line-by-line, for the roAp star 33 Lib.

## 2 THE STAR

33 Lib (=HD 137949) is a cool Ap star with an effective temperature of 7350 K (Ryabchikova et al. 1999) that has been classified earlier as a Cr-Si-Eu star. An effective magnetic

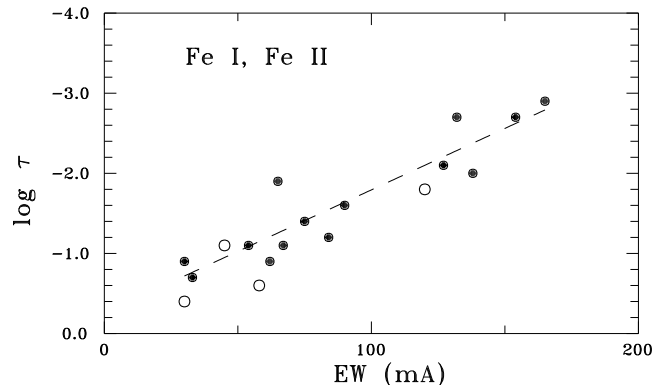


**Figure 2.** The  $W_\lambda - \log \tau$  transformation scale of the model atmosphere of 33 Lib for Fe I (dots) and Fe II (open circles).

field strength of  $\approx +1600$  Gauss has been measured for this star which is only slightly variable (Van den Heuvel 1971; Wolff 1975). Mathys et al. (1997) combined their data and all other available magnetic field measurements for this star and found evidence for a slow increase in the longitudinal field component at a rate of  $\sim 20 \text{ G yr}^{-1}$  which implied a rotational period  $> 75$  years.

The roAp status for this star was established by Kurtz (1982) who found a pulsational period of 8.272 min ( $\nu_1 = 2.01482 \text{ mHz}$ ). This star pulsates in essentially one mode, although Kurtz (1991) found evidence for a second frequency at  $1975 \mu\text{Hz}$  which has yet to be confirmed. That work also detected the second harmonic at  $2\nu_1 = 4.02956 \text{ mHz}$ .

Belmonte et al. (1989) attempted to search for RV variations in 33 Lib using a Fabry-Perot interferometer and a stellar line at  $5317 \text{ \AA}$ . Using more than 6 hours of data they found a peak in the power spectrum at the appropriate frequency and with an amplitude of  $310 \text{ m s}^{-1}$ ; however, due to the high noise level in the power spectrum this result was uncertain.

## 3 OBSERVATIONS

Observations of 33 Lib were made using the 2-d coude spectrograph (Tull et al. 1995) of the 2.7-m telescope at McDonald Observatory on the night of 26 July 1997 between 3:15 UT and 5:26 UT. One focus of the instrument provides a resolving power  $R(=\lambda/\Delta\lambda) = 60,000$  with a nominal wavelength coverage of  $4000\text{--}10,000 \text{ \AA}$  in one exposure when used with a Tektronix  $2048 \times 2048$  CCD detector. Because of the short pulsation period of 33 Lib it was necessary to minimize the time between successive exposures. This was accomplished by binning the CCD by a factor of two perpendicular to the dispersion direction. This halved the detector readout time without sacrificing spectral resolution. A further reduction in readout time was accomplished by framing the CCD so as to record only those pixels on the detector covering the spectral range  $4700\text{--}7000 \text{ \AA}$ . This binning and framing of the CCD resulted in a dead time of 15 secs (CCD readout and data storage). Exposure times were 50 secs resulting in a full duty cycle of 65 secs. Observations

were made continuously one after another resulting in 86 independent observations.

## 4 RESULTS

### 4.1 Broad Band RV Variations

Radial velocities were first computed using each full spectral order as these provided the best RV precision and resulted in a fast determination of the mean RV amplitude over a broad spectral region. Figure 1 shows the Discrete Fourier Transform (DFT) for the RV measurements from each of the spectral orders. The fundamental period, as marked by the vertical dotted line, is present in every spectral order except the one spanning 5878 – 6080 Å.

The measured RV frequencies are all consistent, to within the measurement errors, with the published photometric one. In the analysis that follows we will assume that the 8.272 min period ( $\nu = 2.0148$  mHz =  $174.08$   $\text{cd}^{-1}$ ) is the only one that is present in all the spectral orders. A least squares sine fit was made to the RV amplitude in each spectral order keeping the period fixed at 8.272 min.

Precise stellar radial velocity measurements were made using an iodine absorption cell placed just before the entrance slit of the spectrograph during each observation. This technique is commonly used for measuring precise relative stellar radial velocities and a description of the it can be found elsewhere in the literature (Cochran & Hatzes 1994; Butler et al. 1996). A description of the RV analysis technique as applied to roAp stars can be found in Hatzes & Kürster (1992). Molecular iodine has useful lines in the wavelength range of 5000–6300 Å (14 spectral orders) which dictated the sub-framing of the CCD detector.

The pulsational amplitude ranged from a low of  $7 \text{ m s}^{-1}$  in the spectral order centred on 5928 Å to a high of  $57 \text{ m s}^{-1}$  in orders centred on 5728 Å and 5456 Å. It is also clear from Figure 1 that the pulsational amplitude is not a simple function of wavelength. (We caution the reader that the spectral order whose central wavelength is 5928 Å is contaminated by a plethora of atmospheric water lines and these may affect the RV amplitude derived from the full spectral order.)

### 4.2 RV Amplitude and Phase Variations of Individual Lines

To understand the RV pulsational behavior of 33 Lib as a function of atomic species and line strength we performed an RV analysis on individual spectral lines. The rich spectrum of iodine absorption lines enabled us to do so. Radial velocities were determined over a spectral region containing only a single line. Care was taken to select only unblended lines, although in some cases our analysis was performed on slightly blended lines for which the major contribution to the equivalent width came from one feature. Because of the increased noise level in the RV measurements of individual lines, it was often the case that the dominant peak in the Fourier transform was not always coincident with the photometric frequency. In these instances the statistical significance of the highest peak was assessed using the procedure outlined in Scargle (1982) and Horne & Baliunas

(1986). Of those peaks which did not coincide with the photometric frequency, none were found to be statistically significant (the false alarm probability was always greater than 10%). Thus our line-by-line analysis did not show any conclusive evidence for the presence of an RV frequency that differed from the dominant photometric frequency ( $\nu_1=2.0148$  mHz). Table 1 lists the least squares RV amplitude and relative phases (as a fractional pulsation period) of maximum RV amplitude. The relative pulsation phase was calculated using the time of RV maximum from a least squares fit that was phased with respect to the time of the first observation ( $JD = 2,450,655.6383$ ). In this convention phase 0.88 is near RV maximum. There appears to be significant phase variations for all spectral features that were measured along with a tentative line identification when possible. In our paper line identification were carried out based on line-lists of the Vienna Atomic Line Data base (VALD) (Piskunov et al. 1995), line-list for roAp star HD 122970 (Ryabchikova et al. 2000) and a line-list for Przybylski’s star (Cowley & Mathys 1998). The blends are marked in Table 1 by asterix and their wavelengths and identifications are listed below the primary line.

A major goal of this line-by-line analysis is to develop an approach for deriving both the horizontal and vertical structure to the pulsations. The horizontal effects can be studied if we have a knowledge of the surface distribution of elements on the star. It is well known from Doppler imagery that non-oscillating Ap stars have elements that are inhomogeneously distributed over the stellar surface (Hatzes 1991; Rice & Wehlau 1991,1994). If an element is concentrated in a localized spot, then the cancellation effect for non-radial modes will be smaller for the RV variations from this element. Such a “periodic spatial filter” can be used to derive additional information about the ( $l, m$ ) quantum numbers of the nonradial modes (Mkrtichian 1994). Unfortunately, no Doppler image exists for 33 Lib due to long rotation period and there has been no rotational modulation of spectral features reported for this star. Thus we do not even have crude knowledge as to how elements are distributed on this star.

The study of any vertical structure to the pulsations requires that the acoustic amplitude and phases of a spectral lines be linked to a geometrical depth in the atmosphere. However, unlike for normal stars the effective optical depth of formation of a spectral line cannot be easily linked to a geometric depth in the atmosphere of a roAp stars. The inhomogeneous distribution of elements both horizontally and possibly vertically, as well as the presence of strong magnetic fields complicates the relationship between optical and geometric depths in roAp stars. The optical depth calculated under simple assumptions (e.g. no magnetic fields, no vertical stratification, etc.) may be considered as a very approximate depth scale for the study of vertical atmospheric cross-sections.

As a first approach we decided to link the equivalent widths of the Fe spectral lines,  $W_\lambda$ , with an optical depth,  $\log \tau$ , of the line formation and use this scale for estimating the phase and amplitude distributions throughout the atmosphere. For this approximate  $\log \tau$  scale we assumed that there is no vertical stratification of Fe and other elements in the atmosphere of 33 Lib. This stratification may indeed be present as has been suspected for several elements in Ap stars (Babel & Lanz 1992; Ryabchikova et al. 2002).

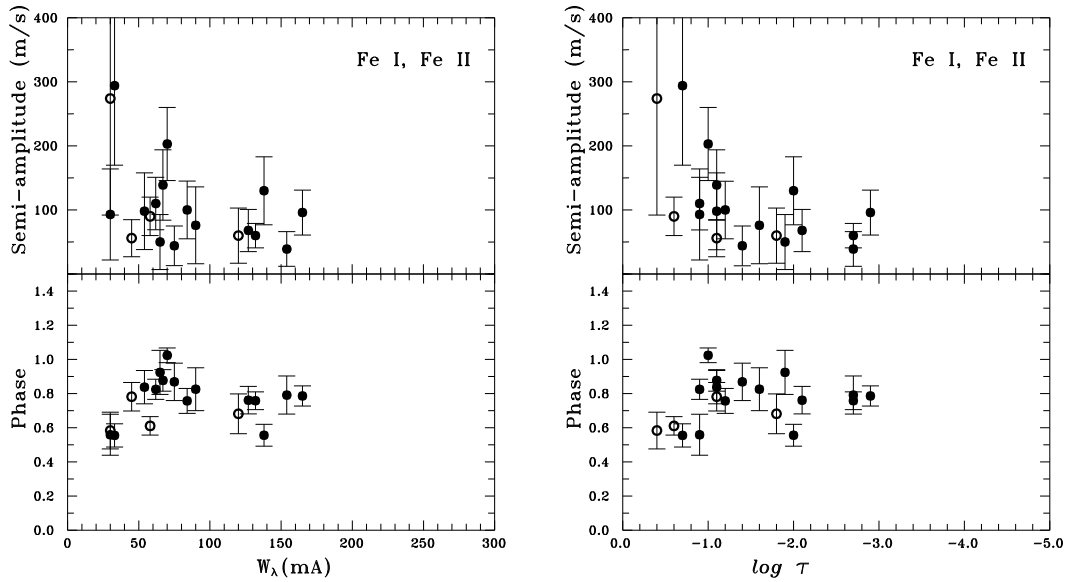


**Figure 3.** The pulsational semi-amplitudes (top panels) and phases as a fractional pulsation period (lower panels) versus line equivalent width (left), and optical depths (right) for Fe lines in 33 Lib. The open circles represent the Fe II while the dots are for Fe I lines. Phases in this and all subsequent figures are in units of fraction of a pulsation period.

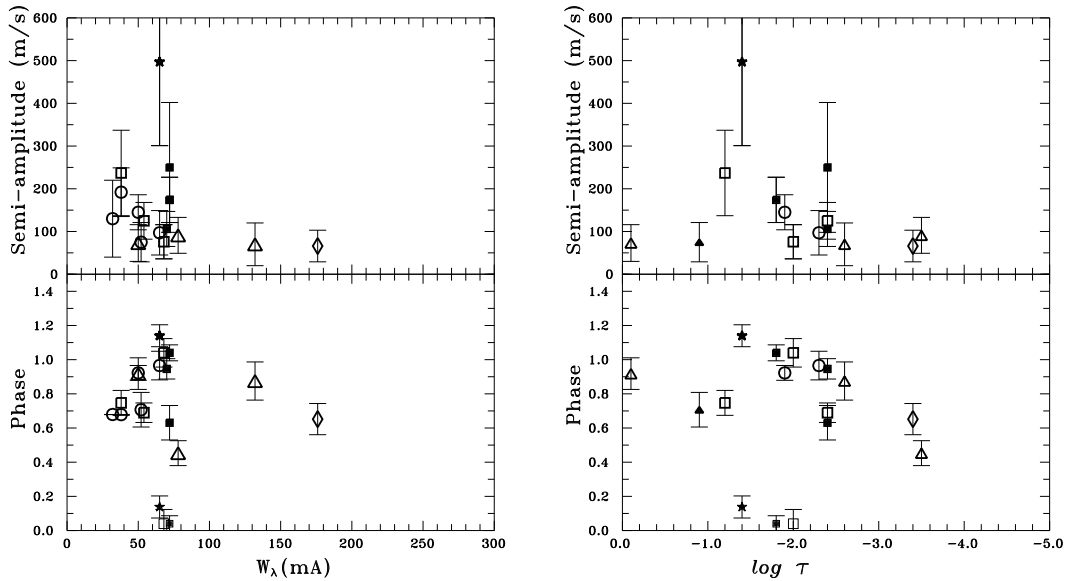


**Figure 4.** The same as in Fig.3 but for Gd II (filled squares), Er II (stars), La (open squares), Ni I (filled triangles), Ca I (open diamonds), Ce II (open circles) and Cr II (open triangles) lines. The 3 lower points near phase 0 have been replotted with phase  $\phi = \phi + 1$ .

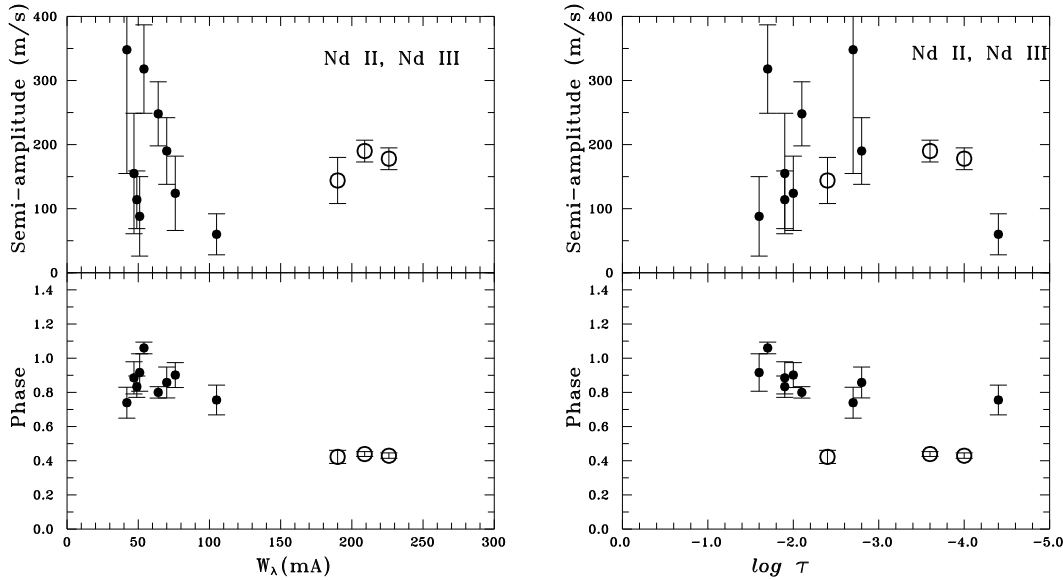


**Figure 5.** The Nd II (dots) and Nd III (open circles) pulsational amplitudes (top left and right panels) and phase (bottom left and right panels) versus equivalent widths (left panels) and approximate optical depths (right panels) in 33 Lib.

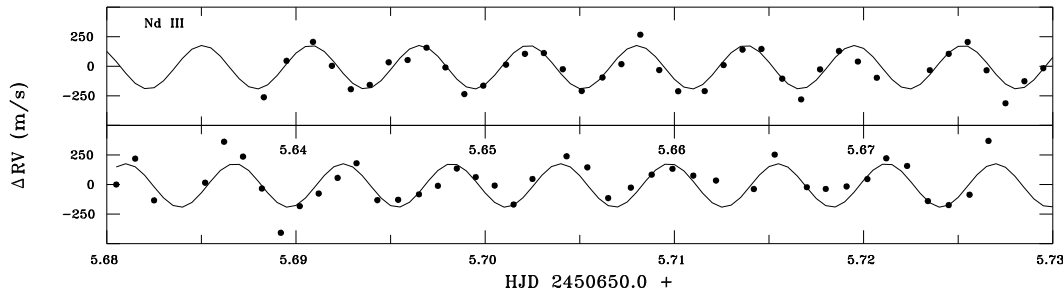


**Figure 6.** The average radial velocity measurements for Nd III 5102.42 Å and Nd III 5294.10 Å (dots). The solid line is sine-wave fit with pulsation period 8.272 min.

Lacking any knowledge of such stratification in 33 Lib this approach seems reasonable at least for Fe since this element is non-peculiar and has approximately a solar abundance in roAp stars (Ryabchikova et al. 2000). This  $\log \tau$  scale for Fe will be used as the standard scale for comparison with acoustic cross-sections using calculated  $\log \tau$  scales of other elements.

The tentative abundance determinations for all unblended lines of elements were done using a version of Kurucz's program WIDTH9 modified by V.V. Tsymbal (Tavrian National University) and A.V. Yushchenko (Odessa National University) so that it could use input files in the VALD format. The optical depths  $\tau$  of spectral line formation were calculated using the SYNTH-NEW code written by V.V. Tsymbal.

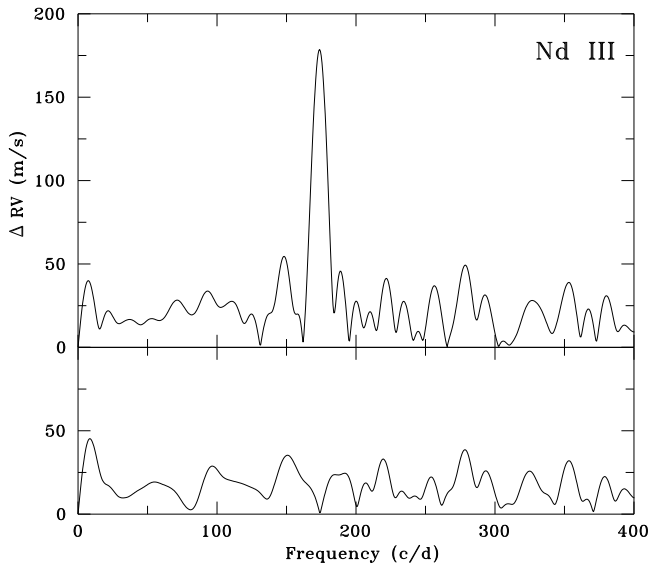
In cases where the atomic data were not present the VALD database (true mostly for rare earth elements), the optical depths were not calculated. For the model atmosphere of 33 Lib we used  $T_{eff} = 7350$  K,  $\log g = 4.4$  (Ryabchikova et al. 1999). The microturbulent velocity of  $\zeta = 2.0 \text{ km s}^{-1}$  was derived by us using the unblended Fe I and Fe II lines.

Figure 2 shows the resulting  $W_\lambda$ - $\log \tau$  dependence for

Fe I (dots) and Fe II (open circles) lines in the range of  $W_\lambda = 30$ – $165$  (mÅ). The dashed line shows the linear fit expressed as  $\log \tau = -0.2132 - 0.01560W_\lambda$  (mÅ). As expected the weaker lines are formed on average deeper in atmosphere than stronger ones.

#### 4.2.1 Fe lines

Figure 3 shows the amplitude,  $K$  (top panels), and phase,  $\phi$  (bottom panels), variation for the Fe lines. (In this and all subsequent figures phases are in units of fraction of a pulsational period.) The panels are divided between those showing  $W_\lambda$  (left) and  $\log \tau$  (right) as the ordinates. The equivalent width is a measured quantity, thus the  $K$ - $W_\lambda$ ,  $\phi$ - $W_\lambda$  plots are model independent. On the other hand the calculated optical depth is dependent on the assumptions used in the model atmosphere. Because roAp stars have large magnetic fields, peculiar abundances, and inhomogeneous temperature and abundance profiles, both horizontally and vertically, the uncertainties in the  $\log \tau$  calculation are larger than for normal stars. The  $W_\lambda$  -  $\log \tau$  mapping could change drastically with improved modeling. For this reason we show figures using both  $W_\lambda$  and  $\log \tau$  as the ordinate.



**Figure 7.** The discrete Fourier transform of the RVs for the Nd III lines shown in Figure 6. The highest peak corresponds to pulsation frequency 174.081 c/d. The lower panel represents the amplitude spectrum of the RV residuals after pre-whitening of this signal.

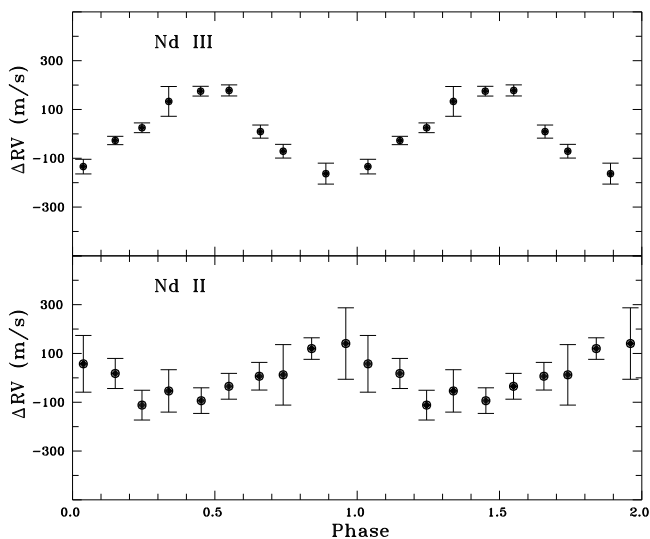


**Figure 8.** The mean radial velocity of Nd III (top panel) and Nd II (bottom panel) lines phased to a pulsational period 8.272 minutes.

There appears to be a weak increase in the pulsation amplitude with decreasing  $W_\lambda$  and increasing  $\log \tau$  for Fe lines. However, the weaker lines also tend to have much larger errors in the amplitude measurement. This trend of increasing amplitude with decreasing line strength may just be an artifact of the larger measurement error for weak lines. Data of better quality is needed to establish this with certainty.

The  $\phi - W_\lambda$ ,  $\phi - \log \tau$  diagrams for Fe lines do show, however, strong evidence for phase variability in the form of a phase jump of  $\Delta\phi \approx 0.3-0.5$  at  $\log \tau \approx -0.9$ .

#### 4.2.2 Rare earths and other elements

Rare earth elements are known to show the largest abundance anomalies and peculiarities in the atmospheres of Ap stars. Due to strong blending in 33 Lib the number of available unblended or partially blended rare earth elements (REE) lines was limited for our analysis (see Table 1.) Figure 4 shows the amplitude (left and right upper panels) and phase (left and right bottom panels) variations respectively for Gd II, Er II, La II, Ce II REE elements, and Ni I, Cr II and Ca I lines. Phase is usually displayed with values between 0 and 1 and with no information on the pulsation cycle. This can influence how one interprets the phase diagram. The lower points (clustered around  $\phi \approx 0$ ) have been replotted at  $\phi \approx 1$ . Doing so makes these points more consistent with the trends shown by the phase of other spectral lines.

The Er II 5454.27 Å line shows the largest pulsation amplitude of 497 m/s ( $S/N=2.54$ ) among measured lines. Again, similar to Fe lines, large errors in the amplitude determinations and small number of lines of REE, Ni, Cr II and Ca I lines prevents us from extracting reliable information about the amplitude dependence with equivalent width.

The spectral features of Gd II, Er II, La II, Ce II, Ni I, Ca I, and Cr II show a decrease in the pulsational phase with decreasing optical depth for  $\log \tau < -1.4$ . There is also the distinct phase jump of  $\Delta\phi \approx 0.4$  at  $\log \tau \approx -1.3$  that may be related to a similar phase jump at  $\log \tau \approx -0.9$  for the Fe lines. If both phase jumps are located at the same geometrical depth in the stellar atmosphere (most likely) then the difference  $\Delta\log \tau \approx -0.4$  in optical depths may be attributed to the distortion of  $\log \tau$  scale due to different spatial (horizontal and vertical) abundance distributions of REE.

We identified a sufficient number of Nd lines to be able to separate these between singly and doubly ionized species. The resulting amplitude and phase dependence versus the  $W_\lambda$  and  $\log \tau$  for Nd II (dots) and Nd III (open circles) lines are given respectively in the left and right panels in Figure 5. The  $K-W_\lambda$  relationship shows an increase in the pulsation amplitude with decreasing  $W_\lambda$  which is not evident in the  $K-\log \tau$  diagrams. Again, large rms amplitude scatter for weak Nd II line prevents us from drawing reliable conclusions about the amplitude changes versus the depth in atmosphere. The phase dependence for Nd II lines shows a slight decrease in the pulsation phase for optical depths smaller than  $\log \tau = -1.6$ .

Three strong Nd III lines 5294.10 Å, 5102.42 Å (partially blended with Nd II 5102.39 Å line) and 6145.07 Å

lines provided RV measurements of exceptional quality. All lines had comparable RV amplitudes and their phases were consistent to within  $\pm 0.005$  of pulsation period. The relatively small scatter in the RV measurements of these lines may be due to the fact that they are formed, on average, in the same atmospheric layers.

The averaged RV measurements for Nd III 5102.42 Å and 5294.1 Å lines as a function of time are shown in Figure 6. Figure 7 shows the DFT amplitude spectrum of these data (top panel). The tallest peak with an amplitude of  $184.3 \text{ ms}^{-1}$  corresponds to known photometric frequency  $\nu_1 = 174.081 \text{ cd}^{-1}$ . The amplitude spectrum of the residuals obtained after pre-whitening the  $174.081 \text{ cd}^{-1}$  signal is shown at bottom panel in Figure 7 and it does not show any peaks above the noise peaks level of  $38 \text{ ms}^{-1}$ . The second harmonic of  $\nu_1$   $\nu_2 = 348.16 \text{ cd}^{-1}$  which is found in the photometric data (Kurtz 1991) with an amplitude ratio  $A(\nu_2)/A(\nu_1) = 0.13$  is not present in the Nd III data above the noise level. If we assume the same ratio of amplitudes of the first and second harmonic for the RV, then the expected RV amplitude of the second harmonic should be about  $24 \text{ ms}^{-1}$  – below our detection limits using radial velocities measured from the strong Nd III lines.

The striking feature about Figure 5 is that the mean phase of the Nd III lines differs by about  $180^\circ$  from the mean phase of the Nd II lines. This is shown more clearly in Figure 8. The bottom panel shows the averaged RV measurements of the four weak Nd II 5456.55 Å, 5614.28 Å, 5625.73 Å and 5761.69 Å lines phased to photometric period. The mean pulsation  $K$ -amplitude of Nd II lines is  $K = 111 \pm 45 \text{ ms}^{-1}$ . The top panel in Figure 8 shows the phased mean radial velocities measured of the two strong 5294.10 Å and 5102.42 Å Nd III lines. The mean  $K$ -amplitude for the Nd III lines is  $175 \pm 10 \text{ ms}^{-1}$ . Clearly, the Nd II and Nd III lines are pulsating almost  $180^\circ$  out-of-phase ( $\Delta\phi = 0.46$ ) with respect to each other.

The lower right panel of Figure 5 shows an obvious discrepancy in the  $\log \tau$  of Nd II and Nd III features. Both ionized species have a comparable range of optical depth, yet their pulsation phases are antiphase. This cannot be the case if both species were formed at the same depth in the atmosphere. This discrepancy can be resolved if the strong Nd III lines were in fact formed much higher in the stellar atmosphere and their calculated (under simplified assumptions about homogeneous vertical elemental distribution) approximate optical depths are essentially overestimated.

Normally, we expect the second ionized species to form in the deep atmospheric layers where the temperature is high or in the outer layers where the pressure is low. The  $\phi - W_\lambda$  diagram (lower left of Figure 5) argues for the former. However, if Nd III lines are indeed formed at much higher layers then this could explain the differences in pulsational phase between Nd II and Nd III and points to the existence of a standing acoustic wave with a node in the upper atmosphere. We could not determine accurately the position of this node because the acoustic cross-sections are not well sampled by spectral lines at small optical depths; we can only estimate the position of this pulsation node as somewhere above  $\log \tau = -4.5$  and that Nd III lines are formed above this node at essentially small  $\log \tau$ . Support for this result also comes from Ryabchikova et al. (2002) who found by a trial-and-error approach in LTE line-profiles synthesis

that Nd is strongly stratified in the atmosphere of  $\gamma$  Equ and it has a thin overabundant (by more than 6 dex) layer above a height  $\log \tau \approx -8.0$ . If a similar vertical stratification of Nd occurs in the atmosphere of 33 Lib, then this would alter the  $\log \tau - W_\lambda$  relationship.

#### 4.2.3 Mean Phase and Amplitude Distributions

Figure 9 shows the amplitude (top panel) and phase (bottom panel) versus optical depths for unblended Fe, Cr, Gd, Er, La, Ce, V, Ca, Ti spectral lines. This  $\log \tau - \phi$  diagram for the majority of unblended lines also shows evidence for the existence of phase variability in acoustic cross-sections. In particular, in addition to the phase jump at  $\log \tau \approx -0.9$  there is also evidence of slow phase changes above  $\log \tau < -0.9$  and below  $\log \tau > -3.0$ .

We also checked whether phase clustering which was found in Fe and REE elements lines was also present in all spectral lines and blends of 33 Lib. The histogram of relative pulsational phases for all lines is shown in Figure 10 (0.05 phase bins) and this shows a clear bi-modal distribution. Most spectral lines are centred on  $\phi = 0.88$  with a spread that is consistent with a Gaussian distribution of half width,  $w = 0.15$ . Nineteen of the spectral lines we examined had a pulsation phase near  $0.425$  or  $164^\circ$  apart from the phase of most other lines. These also appear to have a Gaussian distribution with half-width  $w = 0.07$ . The individual Gaussian distributions are shown as thin lines in the figure while the thick line represents the sum of the two component distributions. The phase  $\phi \approx 0.6$  corresponds to borderline between the two distributions. This bi-modal distribution for 33 Lib is consistent with the Baldry et al. (1998) result for  $\alpha$  Cir. Interestingly, the fraction of our spectral lines having a phase nearly  $180^\circ$  from the mean is about 17%, near the 15% fraction of the bands showing a  $180^\circ$  phase shift in  $\alpha$  Cir found by Baldry et al (1998). The phases of the individual lines have a mean standard deviation of 0.09 which is consistent with the width of the smaller Gaussian. However, the standard deviation of the distribution of phases centred on 0.88 is larger than this by nearly a factor of two. This suggests there is additional variations that cannot be accounted for by the errors of the phase measurements.

The profile of the phase distribution on opposite sides of phase jump  $\log \tau \approx -0.9$  (which is interpreted in §5 as the second acoustic node) seems to contradict the pure standing wave picture which requires a sharp  $180^\circ$  phase jump and non-variable phase on opposite sides of acoustic node.

The phase diagrams of Figures 3, 4, and 9 appear to be a superposition of a step function (i.e. discontinuous jump in phase) along with a linear function of decreasing phase with  $\log \tau$ . That is to say, the phase after (and possibly before) the phase jump at  $\log \tau \approx -1$  is not constant, rather it decreases linearly as one moves outward in the atmosphere (smaller values of  $\log \tau$ ). The running wave component and linear decrease in phase outward in the atmosphere can qualitatively explain the non-equality to  $180^\circ$  in the phase spacing between of centers of distributions of two gaussians in Figure 10.

To establish reliably the presence of running wave component in the atmosphere requires more accurate determinations of the phases than presented in this study.



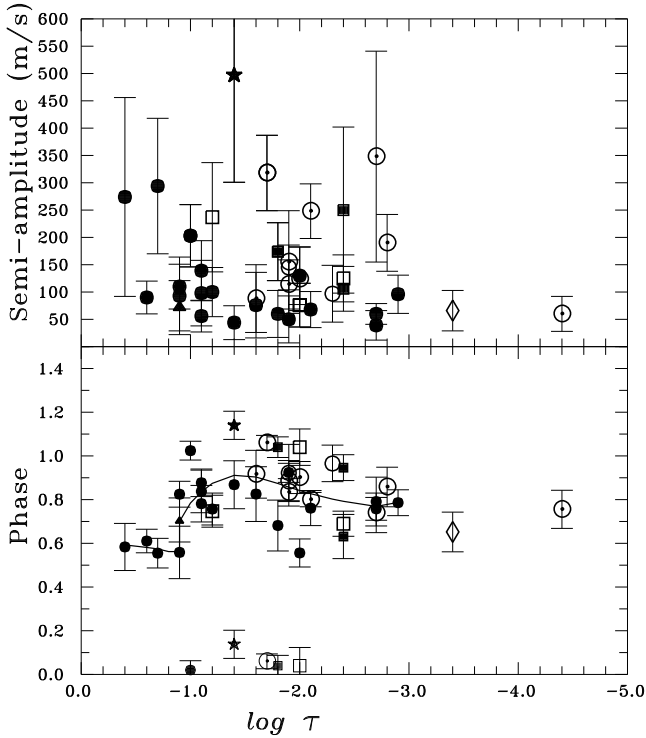


**Figure 9.** The combined acoustic  $K$ - $\log \tau$  (upper panel) and  $\phi$ - $\log \tau$  (bottom panel) cross-sections of atmosphere of 33 Lib for unblended Fe I, Fe II (dots), Gd II (filled squares), La II (open squares), Ce II (open circles), Er II (stars), Ni I (filled triangle), Ca I (diamonds) and Nd II (sun symbols). The solid line in the bottom panel shows polynomial fits to the phase versus  $\log \tau$ . A first order fit was used for  $\log \tau > -0.9$  and ninth order for  $\log \tau < -1.0$ . A phase jump at  $\log \tau \simeq -0.9$  is evident.

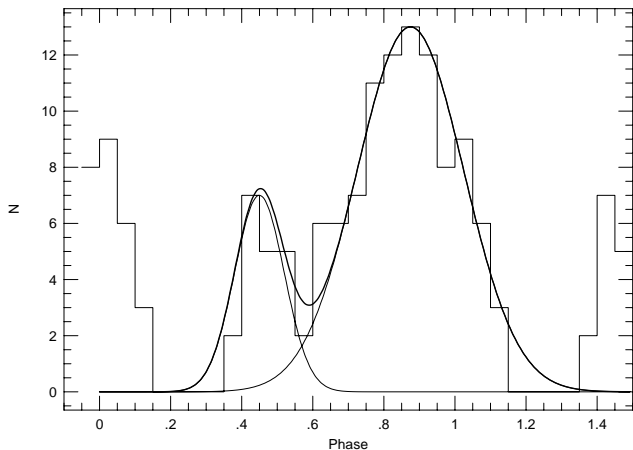


**Figure 10.** Histogram of the distribution of pulsational phases (in fraction of a pulsation period) for all spectral lines. The thin lines represent Gaussian fits to the two distributions with  $\sigma = 0.15$  for the large Gaussian and  $\sigma = 0.07$  for the small Gaussian. The thick line represents the sum of the two component Gaussians. The approximate position of acoustic node is expected at relative  $\phi \simeq 0.6$ .

#### 4.2.4 Effect of the magnetic field

The strong stellar magnetic fields can influence the pulsations in roAp and are believed to cause the high-overtone oblique pulsations with the axis of symmetry coincident with (Kurtz 1990) or close to (Bigot & Dziembowski 2002) the magnetic axis. The magnetic fields can also influence spectral lines through magnetic Zeeman splitting and lead to line broadening and intensification effects which can influence the depth of formation. It was thus natural to investigate whether the pulsational phase or amplitude of spectral lines correlated with their magnetic sensitivity. As a parameter of magnetic sensitivity the effective Lande factors  $g_{eff}$  of spectral line transitions were taken from VALD data base compilation.

We found a puzzling, yet well defined dependence of the pulsation phase with effective Lande  $g$ -factors for some species. Figure 11 shows the pulsational phase versus effective Lande factors  $g_{eff}$  dependencies for Fe I and Fe II, Gd II, La II, Cr II and Ca I lines. The phases are shown over 2 cycles (with the same data points) for better presentation of phase variability.

The relative pulsation phase rises linearly for lines with  $g_{eff} > 0.6$  reaching a maximum at  $g_{eff} \approx 1.05$ . The phase then decreases for  $1.05 < g_{eff} < 1.2$ . Over these intervals the phase variations form what appears to form an inverted ‘V’-shape. There is a discontinuity in the pulsation phase for  $g_{eff} > 1.4$ . The phase variations for these higher  $g_{eff}$ -lines decrease linearly with phase, but are shifted by about 0.5 in phase with respect to the linear trend seen for  $1.1 < g_{eff} < 1.2$ . However, these points can form a continuous phase variation to the lower  $g_{eff}$  lines if one considers that the spectral lines with  $g_{eff} > 1.4$  are actually shifted by one complete pulsational cycle.

The right panel of Figure 11 shows the same diagram as the left panel, but for Nd II, Dy II, Er II and V II lines. These do not show any well defined dependence between phase and effective Lande factors. This discrepancy could be explained by different spatial distributions of these elements in comparison with Fe, Cr, Gd, La and Ca lines. Assuming the presence of a vertical acoustic wave in the atmosphere the pulsation phases variations versus the  $g_{eff}$  for Fe, Cr, Ca, Gd and La lines may be considered as due to the strong influence of magnetic fields on the depth of formation of spectral lines.

According to the acoustic cross-sections of the atmosphere of 33 Lib the vertical scale of the acoustic wave is small and is comparable to the thickness of the line forming region of the stellar atmosphere. The left panel of Figure 11 suggests that magnetic intensification effects introduce changes in the line formation depth that is comparable to the vertical wavelength of the acoustic wave. Thus over this vertical distance there are significant phase changes.

However, the  $g_{eff}$ - $K$  diagram in Figure 12 does not show a correlation between pulsation amplitudes versus the effective Lande  $g$ -factors. A  $g_{eff}$ - $\log \tau$  relationship determined with the inclusion of magnetic effects on the line formation should establish whether the phase changes are due to variability of effective depth of line formation induced by the magnetic sensitivity of lines.

The approximately 2 hour duration of our RV data does not allow us to probe the origin of  $g_{eff}$ - $\phi$  dependence in

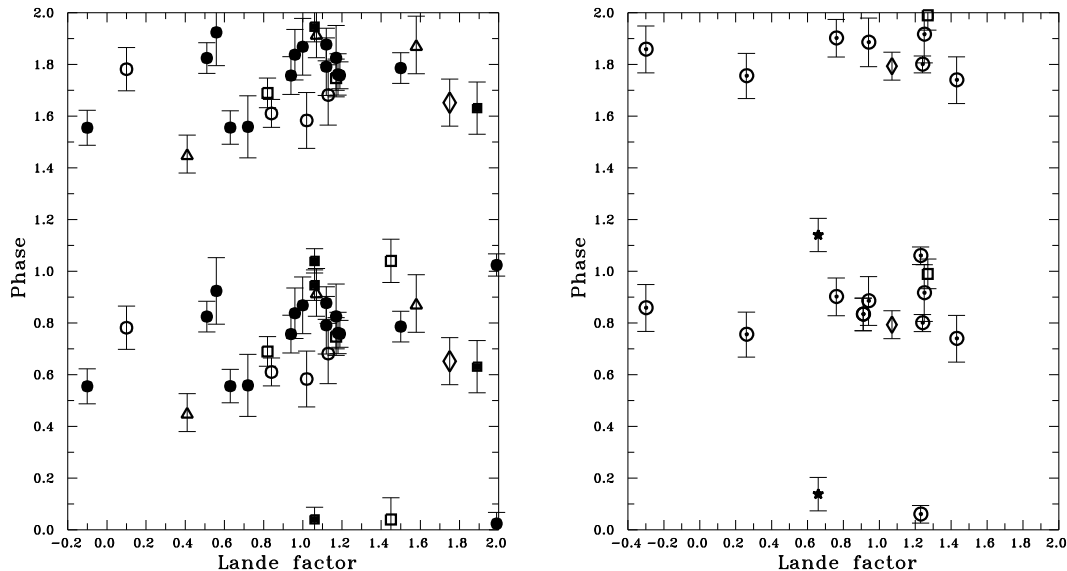


**Figure 11.** The left panel: the pulsation phase (fraction of a period) versus the effective Lande  $g$ -factor for Fe I and Fe II (filled circles), Cr II (open triangles), Gd II (filled squares), La II (open squares) and Ca I (open diamonds). The right panel: the same for Nd II (sun symbols), Dy II (open diamond), Er II (stars), and V II (open square).

33 Lib. Future investigations with more accurate phase and amplitudes determinations and a better description of atmospheric elemental stratifications and magnetic intensification of lines are needed to get a better understanding of this effect.

## 5 DISCUSSION AND CONCLUSIONS

Our pulsational phase data indicate the presence at least one pulsation node in the upper atmosphere, and probably a second one in the deeper atmospheric layers of 33 Lib. The strongest evidence of upper node comes from the RV variations for Nd II and Nd III which are almost  $180^\circ$  out-of-phase with each other (Fig. 8). Since Nd II and Nd III should be formed in different atmospheric layers these data provide convincing evidence for a upper atmospheric pulsational node. We estimate that the node is located above  $\log \tau < -4.5$ .

A second phase jump in the lower atmosphere at  $\log \tau \approx -0.9$  is seen in the weak Fe spectral lines (Fig. 3) and this may be associated with another node. The weak Fe lines with  $\log \tau > -0.9$  oscillate out-of-phase ( $\Delta\phi \approx 0.3$ - $0.5$ ) with those of stronger lines formed at  $\log \tau < -0.9$ . The mean relative phase of these four weak Fe I and Fe II lines is  $\phi \approx 0.6$ , or about the same value that defines the border between the two distributions in Fig. 10. So, we suspect another, lower node below or at  $\log \tau \approx -0.9$  closer to the continuum formation level.

The hypothesis of two acoustic nodes in the atmosphere of 33 Lib can qualitatively explain the  $\approx 17\%$  fraction of spectral lines and blends showing out-of-phase oscillations in Figure 10. According to this hypothesis the upper node is located somewhere above  $\log \tau \approx -4.5$  and the second one below, or at  $\log \tau \approx -0.9$ , closer to the continuum formation level. In this case the layers where the majority of spectral lines are formed are pulsating with relative phases centred

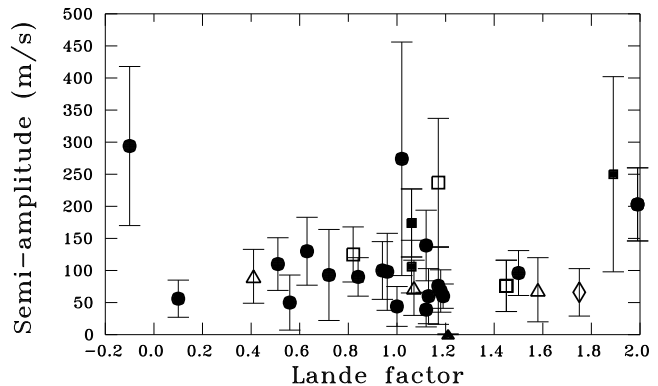


**Figure 12.** The pulsation semi-amplitude versus effective Lande  $g$ -factor for Fe I and Fe II (filled circles), Cr II (open triangles), Gd II (filled squares), La II (open squares), Ca I (open diamonds), and Ni I (filled triangles).

around  $\phi=0.88$  and are between the two nodes. The other spectral lines that contribute to the smaller Gaussian distribution of phases centred on  $\phi=0.425$  are formed in two, out-of-phase pulsating layers: either below the lower node ( $\log \tau > -0.9$ ), where the weaker lines are formed or above the upper node ( $\log \tau < -4.5$ ) where the few Nd III lines and some strong blends are formed.

Theoretical work of Gautschy et al. (1998) supports our hypothesis about two radial pulsation nodes in the atmosphere of an roAp star. Gautschy et al. have calculated a sequence of models for roAp star with a temperature inversion in the upper atmospheric layers. These models predict two displacement nodes in the stellar atmosphere: one close to the continuum formation  $\tau \approx 2/3$  and another at superficial layers (see Fig. 13 in their paper). The location of nodes in atmosphere is model and mode dependent, so the pres-

ence of two nodes in the line forming region is in principle theoretically possible.

The inverted 'V'-shaped variations in pulsational phase with the effective Lande g-factor (Fig. 11) in 33 Lib were unexpected. Stift & Leone (2003) presented an in-depth investigation of the increase in equivalent width of saturated lines under the influence of magnetic fields. Assuming 20 different Zeeman patterns (with the number of components ranging from 3 to 45) they calculated equivalent widths as a function of magnetic field strength and showed that the equivalent width can increase by up to factors of 10. Thus, the magnetic field may strongly affect the in-line absorption and hence the effective depth of formation and this could result in a effective Lande g-factor that is correlated with pulsation phase. This is consistent with phase changes across the atmosphere where the thickness of the line-forming region is comparable to the vertical wavelength of the acoustic wave, and that the influence of the magnetic field through intensification effect also occurs over this small region. Fig. 11 may thus reflect further evidence of a pulsation phase variability and running wave component in the stellar atmosphere. Further investigations of the effective Lande factor  $g_{eff}$  versus pulsation phase in other roAp stars may prove fruitful.

Although RV variations have been measured for relatively few roAp stars, these have already shown a rather complex behavior. In order to interpret fully these variations it is essential to perform detailed spectral analyses of these stars with a special emphasis on the accurate determination of the depth of formation for each spectral line, accurate acoustic cross-sections of atmosphere in lines of different chemical elements, and the study of their variability over the rotation period. This would yield knowledge about the acoustic profiles and location of the radial node in different surface areas and with respect to magnetic axis.

On another hand, the acoustic cross-sections can also be used to refine the atmospheric models. The pulsation phase (and amplitude) distribution across the atmosphere is a unique and true link with the geometrical depth scale and could be used for atmospheric tomography. This tomographic procedure should include the semi-empirical adjustment and tuning of the vertical and horizontal elemental distributions (the latter can be known in advance, from Doppler imaging) and physical conditions in the model of atmosphere until the best solution for phase and amplitude cross-sections versus geometric depths for different chemical elements is attained (and hence true transformation scales between EW, optical and geometrical depths obtained). For example, in our simplified approach for a model atmosphere of 33 Lib with homogeneous vertical distribution of Nd, the calculated optical depths suggest that Nd II and Nd III are formed at comparable optical depths which is inconsistent with the pulsational phases for Nd III (Fig 5).

The restoration of vertical atmospheric structure and geometrical depths of spectral line formation are only as accurate as the measured RV pulsation phases and amplitudes of spectral lines formed in different atmospheric layers. For the long duration (weeks) spectral observations it is possible to increase the resolution in geometrical depths across the line-forming atmosphere to  $10^{-3}$  or better.

Moreover, as the different p-modes having different oscillation frequencies are expected to have different depths for acoustic nodes in atmosphere (Gautschy et al., 1998),

this will lead to the different phase (and amplitude) profiles in atmospheric cross-sections measured on the same spectral lines but on different oscillation frequencies (i.e. different modes). This expected effect gives an independent and additional tool to sounding the vertical acoustic structure of atmosphere and study vertical chemical abundances in multi-mode roAp stars using different cross-sections. Such an accurate tomographic analysis is beyond the scope of the current work and requires longer time series for an mono- or multi-mode roAp star, RV measurements of much larger number spectral lines, and data taken with better signal-to-noise ratio. These data can be used to glean valuable information on the 3-dimensional structure to the pulsations and the stellar atmosphere of roAp stars.

## 6 ACKNOWLEDGEMENTS

This research was supported by grant UP2-317 by the Civilian Research and Development Foundation (CRDF) during 1997-1999 and a grant by the German Academic Exchange Service (DAAD) during 2002. We express our sincerest thanks to T. Ryabchikova for making available to us linelist for roAp star HD 122970. DEM would like thank A. Gautschy for useful comments on his models of roAp stars and V.V. Tsymbal and A.V. Yushchenko for helpful comments on spectral synthesis and analysis codes. DEM acknowledges his work as part of research activity of the Astrophysical Research Center for the Structure and Evolution of the Cosmos (ARCSEC) which is supported by the Korean Science and Engineering Foundation.

## REFERENCES

- Babel, J., Lanz, T. 1992, A&A, 263, 232.  
 Baldry, I.K., Bedding, T.R., Viskum, M., Kjeldsen, H., Frandsen, S. 1998, MNRAS, 295, 33.  
 Belmonte, J.A., Bell, C.R., Leeper, M., Palle, P.L., Pietraszewski, Renton, R.E., & Roca Cortés, T. 1989, A&A, 221, 41.  
 Bigot, L. & Dziembowski, W.A. 2002, A&A, 391, 235  
 Butler, R.P., Marcy, G.W., Williams, E., McCarthy, C., Dosanjh, P., & Vogt, S.S. 1996, PASP, 108, 500.  
 Cochran, W.D. & Hatzes, A.P. 1994, Ap&SS, 212, 281.  
 Cowley, C.R. & Mathys, G. 1998, A&A, 339, 165.  
 Gautschy A., Saio & H. Harsemozer, H., 1998, MNRAS, 301, 31.  
 Hatzes, A.P. 1991, MNRAS, 248, 487.  
 Hatzes, A.P. & Kürster, M. 1994, A&A, 285, 454.  
 Hatzes, A.P., Kanaan, A. & Mkrtichian, D.E., 1999a, 'Precise Stellar Radial Velocities' eds. J.B. Hearnshaw and C.D. Scarfe, ASP Conference Series, 185, 166  
 Hatzes, A.P., Kanaan, A. & Mkrtichian, D.E., 1999b, 'Precise Stellar Radial Velocities' eds. J.B. Hearnshaw and C.D. Scarfe, ASP Conference Series, 185, 183  
 Hatzes, A.P., Mkrtichian, D.E. & Kanaan A., 2000, Proc. NATO-ASI Conf. 'Variable Stars As Essential Astrophysical Tools', NATO Science Series C. vol. 544, ed. C.Ibanoglu, 2000, 405  
 Hatzes, A.P., Mkrtichian, D.E., Kanaan, A. 2002, in IAU Colloquium 185: Radial and Nonradial Pulsations as Probes of Stellar Physics. ASP Conference Series, eds. C. Aerts, T.R. Bedding, & J. Christensen-Dalsgaard, San Francisco, p300.  
 Horne, J.H. & Baliunas, S.L. 1986, ApJ, 302, 757.

- Kanaan, A. & Hatzes, A.P. 1998, ApJ, 503, 848 (Paper I).
- Kochukov O. & Ryabchikova T., 2001, A&A, 374, 615
- Kurtz, D.W. 1982, MNRAS, 200, 807.
- Kurtz, D.W. 1990, ARA&A, 28, 607.
- Kurtz, D.W. 1991, MNRAS, 249, 468.
- Libbrecht, K.G. 1988, ApJL, 330, 51.
- Mathys, G, Hubrig, S., Landstreet, J.D., Lanz, T., & Manfroid, J. A&AS, 1997, 123, 353.
- Matthews, J.M., Wehlau, W.H., Walker, G.A.H., & Yang, S. 1988, ApJ, 324, 1099.
- Medupe, R. & Kurtz, D.W. 1998, MNRAS, 299, 371.
- Mkrtichian, D.E. 1992, in 'Stellar Magnetism', eds. Yu.V. Glagolevskij, I.I.Romanyuk, St. Petersburg, 260.
- Mkrtichian, D.E. 1994, Solar Physics, 152, 275.
- Mkrtichian D. E., Hatzes A.P. & Panchuk V.E., 2000, Proc. NATO-ASI Conf. 'Variable Stars As Essential Astrophysical Tools', NATO Science Series C. vol. 544, ed. C.Ibanoglu, 2000, 405
- Piskunov, N.E. Kupka, F., Ryabchikova, T.A., Weiss, W.W. & Jeffry, C.S. 1995, A&AS, 112, 525.
- Rice, J.B. & Wehlau, W.H. 1991, A&A, 246, 195.
- Rice, J.B. & Wehlau, W.H. 1994, A&A, 291, 825.
- Ryabchikova, T.N., Piskunov, N., Savanov, I., Kupka, F., & Malanushenko, V. 1999, A&A, 343, 229.
- Ryabchikova, T.N., Savanov, I.S., Hatzes, A.P., Weiss, W.W. & Handler, G., 2000, A&A, 357, 981.
- Ryabchikova T.N., Piskunov N., Kochukhov O., Tsymbal V., Mittermayer P., & Weiss W.W., 2002, A&A, 384, 545.
- Scargle, J.D. 1982, ApJ, 263, 835.
- Stift, M. & Leone, F. 2003, A&A, 398, 411.
- Tull, R.G., MacQueen, P.J., Sneden, C., & Lambert, D.L. 1995, PASP, 107, 251.
- Van den Heuvel, E.P.J. 1971, A&A, 11, 461.
- Wolff, S.C. 1975, ApJ, 202, 127.

Measured $\lambda$ Å	Identification Å	$W_\lambda$ mÅ	$K$ Amplitude (m/s)	Error (m/s)	Phase	Error	$\log \tau$	$g_{\text{eff}}$
5037.81	5037.78 Ce II	65	97	52	.97	.08	-2.3	0.84
5048.01*	5048.05 La II	38	237	100	.75	.07		
	5048.06 Ni II							
5061.08*	5061.06 Gd II	45	86	74	.51	.13		
	5061.08 Ni II							
	5061.09 Fe II							
5065.07*	5065.01 Fe I	126	61	47	.45	.12		
	5065.03 Fe II							
	5065.04 Cr I							
5070.97	5071.01 Gd II	72	250	152	.63	.10	-2.4	1.89
5082.30	5082.34 Ni I	52	75	46	.71	.10	-0.9	1.21
5092.29*	5092.25 Ti I	76	184	97	.98	.08		
	5092.25 Mo I							
	5092.25 Gd II							
5102.50*	5102.42 Nd III	209	190	17	.44	.01	-3.6	0.47
	5102.39 Nd II							
5105.21	5105.23 Nd II	42	348	193	.74	.09	-2.7	1.43
5121.70*	5121.64 Fe I	60	112	43	.92	.06		
	5121.56 Ni I							
5127.94	5127.87 Fe II	58	90	30	.61	.05	-0.6	0.84
5133.78*	5133.69 Fe I	176	137	45	.95	.05		
	5133.83 Er II							
5171.59*	5171.60 Fe I	125	91	30	.72	.06		
	5171.64 Fe II							
	5171.67 Fe I							
5182.59	5182.59 Nd II	70	190	52	.86	.09	-0.291	-0.3
5183.56*	5183.42 La II	279	45	31	.90	.11		
	5183.60 Mg I							
	5183.71 Ti II							
5188.76*	5188.68 Ti II	240	64	21	.90	.05		
	5188.90 Er II							
5196.51*	5196.48 Cr I	90	141	75	.56	.09		
	5196.59 Cr I							
	5196.592 Mn I							
5197.64*	5197.58 Fe I	125	68	63	.04	.14		
	5197.48 Fe II							
	5197.66 Dy II							
5208.54*	5208.42 Cr I	284	46	21	.07	.07		
	5208.59 Fe I							
5223.25	5223.19 Fe I	62	110	41	.82	.06	-0.90	0.51
5228.37*	5228.37 Fe I	65	86	39	.88	.07		
	5228.40 Fe I							
	5228.42 Nd II							
5232.92*	5232.92 Ce II	170	42	32	.06	.12		
	5232.95 Fe I							
5242.48	5242.49 Fe I	75	44	31	.87	.11	-1.4	1.0
5246.78	5246.77 Cr II	132	70	50	.88	.11	-2.6	1.58

**Table 1.** Radial Velocity Amplitudes. All phases are in fraction of a pulsational period.

Measured $\lambda$ Å	Identification Å	$W_\lambda$ mÅ	$K$ Amplitude (m/s)	Error (m/s)	Phase	Error	$\log\tau$	$g_{eff}$
5252.02*	5252.03 Ce I 5252.02 Ti II 5252.10 Ti I	115	126	68	.37	.08		
5257.05*	5257.02 Er II 5256.94 Fe II	140	55	54	.39	.15		
5261.66*	5261.70 Ca I 5261.76 Cr I	130	22	21	.80	.16		
5269.51*	5269.48 Nd II 5269.52 Ce II 5269.54 Fe II	146	72	65	.64	.15		
5273.39*	5273.37 Fe I 5273.43 Nd II	140	70	52	.00	.11		
5278.20*	5278.20 Fe II 5278.25 Cr I	61	96	68	.95	.054		
5281.78	5281.79 Fe I	127	68	33	.76	.08	-2.1	1.18
5290.81	5290.82 La II	54	125	43	.69	.06	-2.4	0.82
5294.10	5294.10 Nd III	226	178	17	.43	.02	-4.0	0.9
5307.23*	5307.23 Ca II 5307.27 Cr I 5307.36 Fe I	143	9	27	0.79	0.47		
5316.65*	5316.60 Nd II 5316.62 Fe II 5316.78 Fe II	250	75	26	.73	.06		
5319.79	5319.82 Nd II	105	60	32	.76	.09	-4.4	0.26
5324.17	5324.18 Fe I	165	96	35	.79	.06	-2.9	1.5
5325.56	5325.55 Fe II	120	60	43	.68	.12	-1.8	1.13
5334.21*	5334.23 Er II 5334.24 Sc II	113	131	62	.97	.07		
5334.84*	5334.87 Cr II 5334.87 Mn II	78	91	42	.45	.07	-3.5	0.41
5362.86*	5362.87 Fe II 5362.77 Co I	156	61	46	.92	1.17		
5364.87	5364.87 Fe I	138	130	53	.56	.06	-2.0	0.63
5373.01	5373.01 Tm II	50	93	64	.50	.11		
5373.70*	5373.71 Fe I 5373.72 Cr I	75	117	92	.96	.12		
5379.19	uncl	42	182	88	.83	.08		
5383.37	5383.37 Fe I	154	39	27	.79	.11	-2.7	1.12

**Table 1.** Radial Velocity Amplitudes (cont.)

Measured $\lambda$ Å	Identification Å	$W_\lambda$ mÅ	$K$ Amplitude (m/s)	Error (m/s)	Phase	Error	$\log\tau$	$g_{eff}$
5395.20	5395.22 Fe I	33	294	124	.55	.07	-0.7	-0.1
5395.82*	5395.75 Cr II	32	139	36	.89	.04		
	5395.90 Er II							
	5395.63 Cr II							
	5395.86 Fe II							
5402.78*	5402.76 Eu I	56	92	41	.78	.08		
	5402.77 Y II							
5407.59*	5407.60 Cr II	104	140	45	.87	.05		
	5407.42 Mn I							
	5407.48 Fe I							
5429.74*	5429.50 Fe I	312	35	39	.41	.17		
	5429.70 Fe I							
	5429.83 Fe I							
5439.72	5439.71 Fe II	30	274	182	.58	.11	-0.40	1.02
5442.29*	5442.26 Nd II	75	100	63	.61	.10		
	5442.37 Cr I							
5451.13*	5451.12 Nd II	93	207	65	.85	.05		
	5451.13 Ce II							
5454.24	5454.27 Er II	65	497	196	.14	.06	-1.4	0.66
5455.49*	5455.44 Fe I	282	160	49	.83	.05		
	5455.47 Dy II							
5456.55	5456.55 Nd II	51	88	62	.92	.11	-1.6	1.25
5468.34	5468.37 Ce II	50	145	41	.92	.04	-1.9	1.31
5469.12	5469.10 Dy II	53	133	45	.79	.05	-	1.07
5471.42		50	149	74	.45	.08		
5482.30	5482.27 La II	68	76	40	.04	.08	-2.0	1.45
5487.65*	5487.63 Mn I	188	32	25	.95	.13		
	5487.74 Fe I							
	5487.76 Fe I							
5513.44*	5513.39 Fe I	80	136	46	.00	.05		
	5513.56 Pr II							
5525.109	5525.13 Fe II	45	56	29	.78	.08	-1.1	0.1
5533.79*	5533.79 Nd I	32	101	55	.84	.09		
	5533.82 V I							
5543.15*	5543.15 Fe I	100	110	35	.75	.05		
	5543.04 Cr II							
5554.87*	5554.89 Fe I	90	58	35	.64	.10		
	5554.95 Cr I							
5557.90*	5557.91 Fe I	80	133	55	.91	.06		
	5557.98 Fe I							
5567.75*	5567.75 Mn I	54	102	62	.73	.10		
	5567.84 Fe II							
5569.07	5569.08 Cr II	50	73	43	.92	.09	-0.1	1.07

**Table 1.** Radial Velocity Amplitudes (cont.)

Measured $\lambda$ Å	Identification Å	$W_\lambda$ mÅ	$K$ Amplitude (m/s)	Error (m/s)	Phase	Error	$\log\tau$	$g_{eff}$
5586.09*	5586.05 Cr II 5586.08 V I 5586.13 Gd II	55	163	58	.89	.06		
5586.75	5586.76 Fe I 5586.84 Cr I	130	76	30	.70	.07		
5588.92*	5588.75 Ca I 5588.93 Nd II	140	44	21	.64	.08		
5594.55*	5594.46 Ca I 5594.42 Nd II 5594.65 Fe I	188	70	46	.84	.10		
5602.84*	5602.85 Ca I 5602.66 Nd II 5602.77 Fe I 5602.88 Si I 5602.94 Fe I	230	16	30	.94	.28		
5614.20	5614.28 Nd II	47	155	94	.89	.09	-1.9	0.94
5615.58*	5615.64 Fe I 5615.30 Fe I 5615.62 Fe I	132	60	19	.76	.05	-2.7	1.19
5620.54*	5620.49 Fe I 5620.59 Nd II 5620.63 Cr II	121	109	40	.74	.06		
5625.63	5625.73 Nd II	76	124	58	.90	.07	-2.0	0.76
5626.63*	5626.73 Ce II 5626.53 Er II 5626.73 Fe II	77	147	43	.01	.05		
5630.35	5630.38 Ce II	38	192	57	.02	.05		
5637.47*	5637.36 Ce II 5637.30 Sm II	85	77	41	.79	.09		
5638.33*	5638.27 Fe I 5638.16 Cr I	67	139	55	.88	.06	-1.1	1.12
5640.45	uncl	30	75	58	.42	.12		
5641.61*	5641.69 Cr I 5641.50 Dy II	109	70	48	.94	.11		
5650.32	uncl	48	69	32	.89	.07		
5658.42*	5658.53 Fe I 5658.36 Sc II	150	4	21	.61	.84		
5678.46*	5678.39 Cr II 5678.61 Cr I	167	286	113	.49	.06		
5679.56	5679.59 Sm II	70	160	59	.05	.06		
5680.22*	5680.26 Ce II 5680.24 Fe I	70	22	33	.73	.24		

**Table 1.** Radial Velocity Amplitudes Lines (cont.)



Measured $\lambda$ Å	Identification Å	$W_\lambda$ mÅ	$K$ Amp. (m/s)	Error (m/s)	Phase	Error	$\log\tau$	$g_{eff}$
5691.48*	5691.46 Ce II 5691.48 Ni I 5691.50 Fe I	32	188	67	.16	.06		
5721.96	5721.96 Gd II	72	174	53	.04	.05	-1.8	1.06
5753.09*	5753.12 Fe I 5753.02 Pr II	84	100	45	.76	.07	-1.2	0.94
5757.65	5757.63 Er II	61	214	66	.98	.05		
5761.62	5761.69 Nd II	49	114	45	.83	.06	-1.9	0.91
5763.00*	5762.99 Fe I 5762.99 Ce II 5762.98 Si I	122	70	39	.88	.09		
5804.07*	5804.00 Nd II 5804.03 Fe I	103	175	48	.81	.04		
5834.07	5833.93 Fe I	70	203	57	.02	.04	-1.0	1.99
5835.45*	5835.49 Fe II 5835.42 Fe I	35	165	53	.63	.06		
5859.67*	5859.58 Fe I 5859.67 Pr II	93	52	27	.91	.08		
5998.90	5998.94 Pr III	109	105	64	.21	.10		
6004.62	6004.56 Gd II	70	106	41	.95	.06	-2.4	1.06
6014.54	uncl	76	125	61	.50	.07		
6024.05	6024.06 Fe I	90	76	60	.83	.13	-1.6	1.17
6027.03*	6027.05 Fe I 6027.05 Cr II	54	98	60	.84	.10	-1.1	0.96
6034.18*	6034.23 Nd II 6034.21 Ce II	64	248	50	.80	.03	-2.1	1.24
6051.85*	6051.86 Nd II 6051.80 Ce II	54	318	69	.06	.03	-1.7	1.23
6065.49	6065.48 Fe I	65	50	43	.92	.13	-1.9	0.68
6122.29	6122.22 Ca I	176	66	37	.65	.09	-3.4	1.75
6127.90	6127.91 Fe I	30	93	71	.56	.12	-0.9	0.72
6136.62*	6136.61 Ti I 6136.62 Fe I 6136.63 Cr I	90	104	87	.45	.13		
6140.30	6140.22 Ce II	32	130	90	.07	.11		

**Table 1.** Radial Velocity Amplitudes (cont.)

Measured $\lambda$ Å	Identification Å	$W_\lambda$ mÅ	$K_o$	Amplitude (m/s)	Error (m/s)	Phase	Error	$\log\tau$	$g_{eff}$
6141.71*	6141.71 Ba II	130		198	92	.11	.07		
	6141.73 Fe I								
6145.05*	6145.07 Nd III	190		144	36	.42	.04	-2.4	
	6145.02 Si I								
6147.75*	6147.74 Fe II	115		168	85	.81	.08		
	6147.83 Fe I								
6230.75*	6230.72 Fe I	80		440	120	.83	.04		
	6230.80 V I								

**Table 1.** Radial Velocity Amplitudes (cont).